Materials Letters 298 (2021) 130006

Contents lists available at ScienceDirect

Materials Letters

journal homepage: www.elsevier.com/locate/mlblue

Candle flame fabrication of carbon coated CuO-Cu_2O composite photocathode for photoelectrochemical water reduction

Chunyu Xiao, Bo Lei, Weiliang Jin, Lingling Xu *

Key Laboratory of Photonic and Electronic Bandgap Materials, Ministry of Education, School of Physics and Electronic Engineering, Harbin Normal University, Harbin 150025, China

ARTICLE INFO

Article history:
Received 4 March 2021
Received in revised form 20 April 2021
Accepted 1 May 2021
Available online 9 May 2021

Keywords:
Photoelectrochemical water splitting
Photocathode
Composite materials
CuO-Cu_2O
Candle flame

ABSTRACT

In this work, carbon coated-CuO-Cu_2O composite on copper foam (C-CuO-Cu_2O/CF) is synthesized by candle flame treatment and is evaluated as a photocathode of photoelectrochemical water splitting (PEC). The photocurrent density of C-CuO-Cu_2O/CF electrode can reach −1.2 mA cm^{-2} (at 0 V vs. RHE), which is about 12 times higher than that of Cu_2O/CF. The high PEC performance is due to the carbon modification and the unique composition which increase the carrier concentration and reduce the carrier recombination rate and promote charge transfer at electrode-electrolyte interface. Our results proves that candle flame annealing is a promising way for the rational design of carbon modified photoelectrodes.

1. Introduction

Hydrogen fuel occupies an important position in renewable and sustainable development due to its high calorific value and zero pollution. Photoelectrochemical (PEC) water splitting is an effective way for hydrogen generation and its efficiency is greatly dependent on the photoelectrodes. As for photocathode, cuprous oxide (Cu_2O) has attracted great attention due to its small band gap, high earth abundance, and strong light absorption ability [1–3]. However, the problems such as insufficient light absorption, fast recombination of photo-generated charges significantly restrict the performance of Cu_2O photocathode [4,5]. In order to solve these problems, a rational design of CuO/Cu_2O composite can effectively enhance carriers separation rate [5,6]. Moreover, Yu et al. designed a carbon layer coated Cu_2O photoelectrode via the glucose carbonization and the good conductivity of carbon layer played an effective role to improve Cu_2O activity [7]. Liu et al. found that the light absorption of $CaFe_2O_4$ electrode can be enlarged into the visible light region, and the transfer of photocarriers was enhanced after the surface coating of carbon [8]. Although the role of carbon protection and the CuO/Cu_2O composite structure have been discussed for the enhancing the photoelectrochemical efficiency, only few studies have been reported on the construction of carbon decorated CuO/Cu_2O electrodes [9].

In this work, carbon coated CuO-Cu_2O composite on CF (C-CuO-Cu_2O/CF) was fabricated by a fast and easy candle combustion method. As-obtained hybrid electrode exhibited greatly enhanced conductivity and photoelectrochemical activity, making it a very promising photocathode for PEC application.

2. Experimental

2.1. Preparation of C-Cu_2O/CF and C-CuO-Cu_2O/CF

Cu_2O/CF was firstly fabricated via the hydrothermal method and detailed information was shown in Supplementary data. A candle bought from IKEA was used to synthesize C-Cu_2O/CF and C-CuO-Cu_2O/CF electrodes using Cu_2O/CF as precursor. Before treatment, a candle was firstly lighted and burned for 1 min. Then, the precursors were positioned ~1 cm and 4 cm away from the candle flame for 5 s to fabrication C-CuO-Cu_2O/CF and C-Cu_2O/CF, respectively.

2.2. Characterization

X-ray diffraction (XRD) measurement was operated on a Rigaku RU-D/max 2500 X ray diffractometer with Cu Kα radiation (40 kV, 30 mA). Raman spectra were collected by a Horiba HR-800 confocal Raman spectrometer with an Ar^+ laser (514.5 nm). A scanning electron microscope (SEM, Hitachi SU-70, 15 kV) and a transmission electron microscope (TEM, FEI-Tecnai F20) were performed to characterize the sample morphology and microstructure.

* Corresponding author.
E-mail address: xulingling_hit@163.com (L. Xu).

https://doi.org/10.1016/j.matlet.2021.130006
0167-577X/

2.3. Photoelectrochemical measurements

All photoelectrochemical tests were performed by an electrochemical workstation (CHI 760E) in 0.5 M Na_2SO_4 electrolyte. The photoelectrochemical (PEC) properties were measured under a 300 W Xe lamp in a three-electrode configuration. A saturated calome electrode (SCE), a Pt foil and copper foam samples were employed as reference, counter and working electrodes, respectively. For chopped linear sweep voltammograms (LSV) measurement, the voltage was scanned from 0 to 0.5 V_{RHE} at a speed of 10 mV/s. Electrochemical impedance spectra (EIS) were measured at 0.4 V_{RHE} under illumination within the frequency range of 10 kHz–0.1 kHz. The Mott-Schottky (M-S) curves were collected in dark at 1000 Hz. The incident photon to current conversion efficiency (IPCE) was recorded at 0 V_{RHE} using a Xe lamp with a monochromator at each single wavelength.

3. Results and discussion

The crystal phases of as-prepared samples were determined by using XRD and the patterns are provided in Fig. 1a. For hydrothermal growth precursor, in addition to strong diffraction peaks of Cu substrate (JCPDS No.85-1326), the diffraction peaks at 2θ of 29.6, 36.5, 42.3, 61.4 and 73.5° can be respectively assigned to (110), (111), (200), (220) and (311) planes of Cu_2O (JCPDS No. 78-2076). Similar profile is obtained for C-Cu_2O/CF with no additional peaks presented. While for C-CuO-Cu_2O/CF, two extra weak peaks are detected, which can be attributed to (−111), (111) planes of CuO (JCPDS No. 80-1916). Raman measurement was carried out to further confirm phases and the presence of carbon. As shown in Fig. 1b, peaks at 215, 289, 415 and 640 cm^{-1} can be ascribed to Cu_2O in Cu_2O/CF. After the candle annealing, two prominent peaks at 1368 cm^{-1} and 1592 cm^{-1} can be found in C-Cu_2O/CF and C-CuO-Cu_2O/CF, which are typical D band and G band of carbon, respectively [6,8]. This observation clearly confirms the successful deposition of carbon after the candle annealing. Compared with C-Cu_2O/CF, the intensities of D and G bands are much stronger in C-CuO-Cu_2O/CF, suggesting higher amount of carbon is deposited on the CuO-Cu_2O surface. Moreover, the Raman peaks of Cu_2O in C-CuO-Cu_2O/CF turns to be weak, while a new small peak at 286 cm^{-1} can be detected, suggesting the formation of CuO [10,11].

Fig. 1c shows a SEM image of Cu_2O/CF precursor, where the staggered large blocks are uniformly covered on copper substrate with regular edges and smooth surface. Furnace heated CuO-Cu_2O/CF shows similar morphology (Fig. S1). After carbon deposition (Fig. 1d), the morphology of C-Cu_2O/CF remains almost the same as that of Cu_2O/CF, except for many flocculent soots on the surface. Fig. 1e and f present the morphology of C-CuO-Cu_2O/CF, where lots of cube blocks are formed with small holes decorated on the surface. Moreover, flocculent matter can also be observed on the surface, which are considered as the carbon deposition as evidenced by Raman spectra in Fig. 1b. Furthermore, small holes formed during annealing can provide abundant reaction sites on the electrode, which would be beneficial to the performance improvement.

A low resolution TEM image of C-CuO-Cu_2O/CF in Fig. 2a reveals that the electrode surface is uniform covered by a layer of fluffy matter, which is confirmed as carbon from the high resolution TEM image in Fig. 2b. The lattice fringe of carbon ordered in short-range is similar with the reported results obtained via candle combustion [12]. The Invert Fast Fourier Transformation (IFFT) images in Fig. 2c reveal two plane spacings of 0.15 and 0.21 nm that can be well assigned to (−113) plane of CuO and (200) plane of Cu_2O, respectively. These are also supported by the diffraction rings in Fig. 2d. Thus, based on XRD, Raman, SEM and TEM results, the successful construction of C-CuO-Cu_2O/CF electrode on conductive CF support is confirmed.

The chopped LSV curves are shown in Fig. 3a, the photocurrent density of Cu_2O/CF is about −0.04 mA cm^{-2} @0 V V_{RHE}.

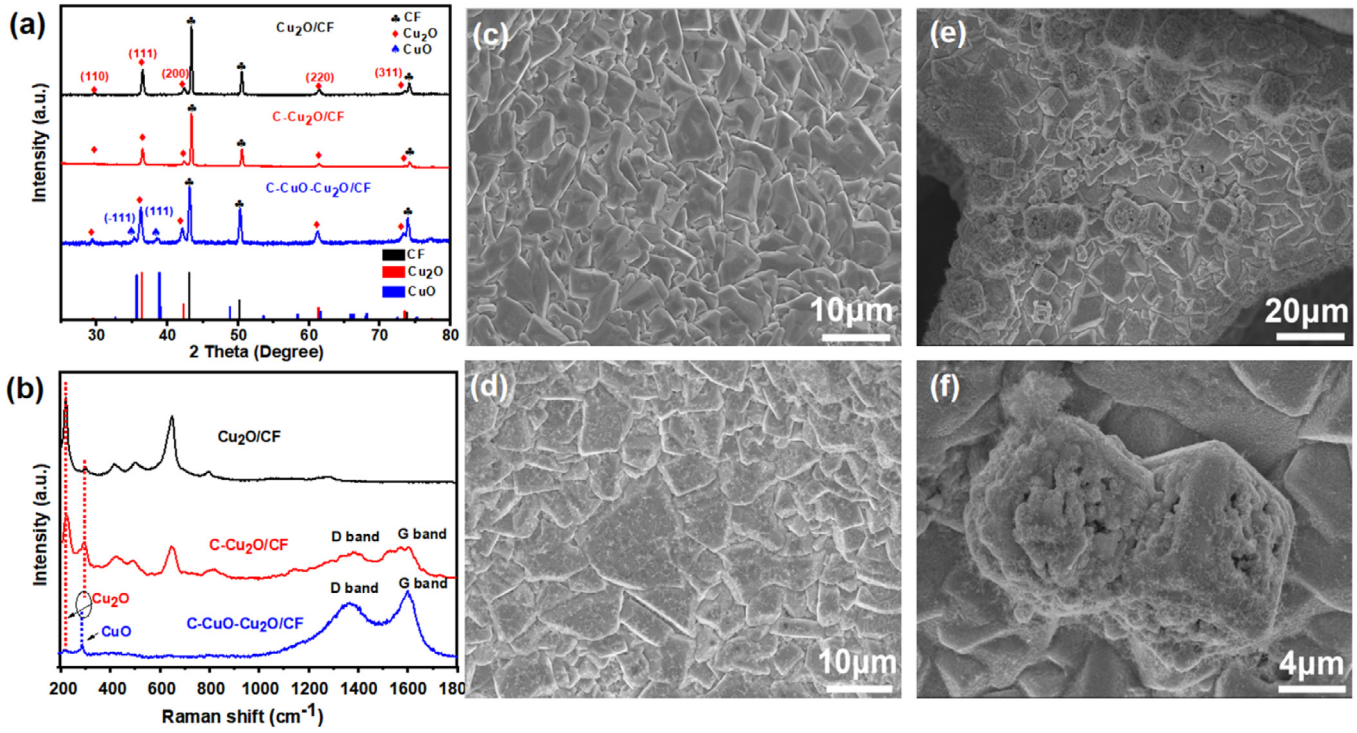

Fig. 1. (a) XRD patterns of Cu_2O/CF, C-Cu_2O/CF and C-CuO-Cu_2O/CF, (b) Raman spectra of C-Cu_2O/CF and C-CuO-Cu_2O/CF electrodes. SEM images of (c) Cu_2O/CF, (d) C-Cu_2O/CF, (e) overview and (f) enlarged view of C-CuO-Cu_2O/CF.

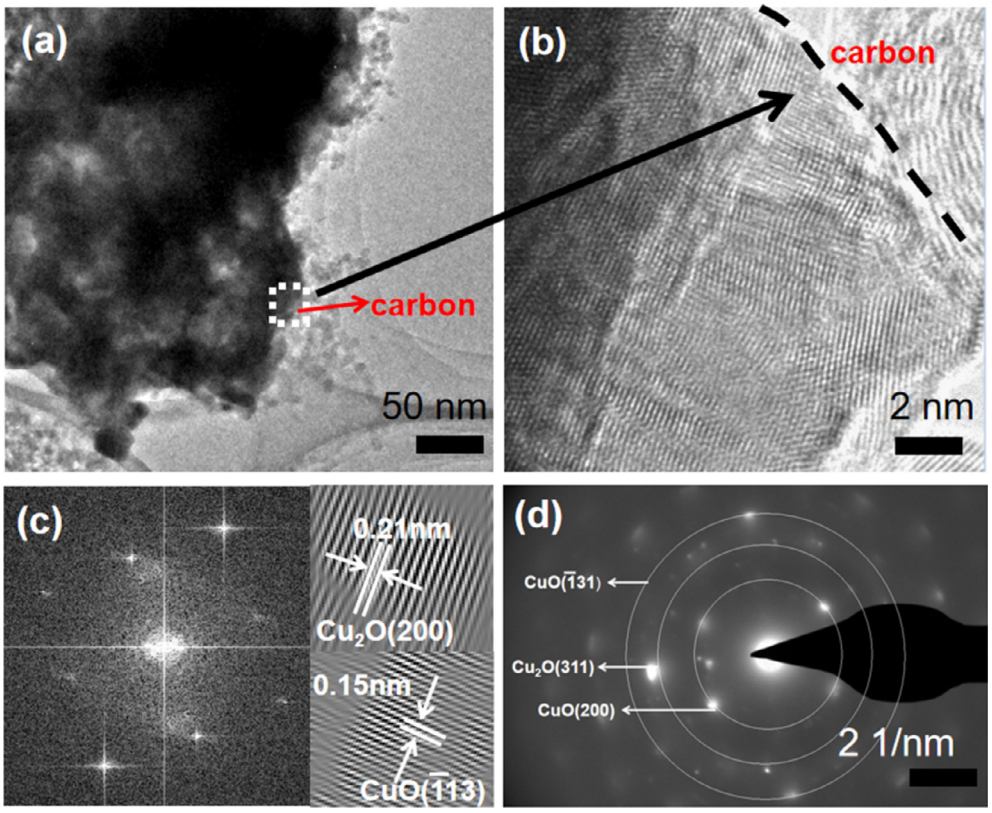

Fig. 2. (a) TEM image, (b) HRTEM image, (c) SAED pattern and (d) Diffraction rings of C-CuO-Cu_2O/CF electrode.

After the carbon deposition, the photocurrent density of C-Cu_2O/CF is slightly improved to −0.1 mA cm^{-2} @0 V_{RHE}. It is because the carbon will accelerate the transfer rate of carriers at the interface [13]. As for the C-CuO-Cu_2O/CF electrode, the maximum photocurrent density can reach −1.2 mA cm^{-2} @0 V V_{RHE}, nearly twelve times larger than that of C-Cu_2O/CF. Mott-Schottky measurement was performed to determine the carriers concentration (N_D). As shown in Fig. 3b, the N_D values derived from the curves for Cu_2O/CF, C-Cu_2O/CF, CuO-Cu_2O/CF and C-CuO-Cu_2O/CF are 1.83 × 10^{20}, 1.90 × 10^{20}, 2.01 × 10^{20} and 2.28 × 10^{20} cm^{-3}, respectively. Clearly, the C-CuO-Cu_2O/CF electrode exhibits the highest carrier concentration, indicating CuO and carbon phases can improve the carrier transfer. The charge transfer performance is further studied by electrochemical impedance spectra. As-collected Nyquist plots and an equivalent circuit are shown in Fig. 3c. The diameter of semicircle for C-CuO-Cu_2O/CF is smaller than the other three electrodes. The charge transfer resistance (R_{ct}) values are determined as 612, 1627, 799 and 1544 Ω for C-CuO-Cu_2O/CF, CuO-Cu_2O/CF, C-Cu_2O/CF and Cu_2O/CF electrodes, respectively. The lowest R_{ct} value of C-CuO-Cu_2O/CF proves the deposited carbon promotes electrons transportation from CuO-Cu_2O to the electrolyte. The accelerated charge transfer speed will then enhance the PEC performance of hybrid photocathode.

The incident photon-to-current conversion efficiency (IPCE) was measured under the incident light (Fig. 3d). The highest IPCE value of C-CuO-Cu_2O/CF probably can be attributed to the formation of CuO that greatly inhibits photocarriers recombination and accelerates the electron and hole transport to electrolyte. Moreover, the photoconversion efficiency improvement is consistent with the increased concentration of carriers as confirmed by M-S measurement.

4. Conclusion

Carbon coated-CuO-Cu_2O hybrid photocathode on conductive CF was successfully synthesized by a facile candle flame treatment. This electrode exhibited greatly enhanced photoelectrochemical activity with a photocurrent density of −1.2 mA cm^{-2} at 0 V_{RHE}. Its high performance is attributed to the unique surface carbon coating and CuO-Cu_2O interface, which can increase the carrier concentration and reduce the carrier recombination rate and enhance charge transfer at the interface of photocathode/electrolyte, as proved by M-S, IPCE and EIS results. The significantly enhanced activity enables C-CuO-Cu_2O/CF as an attractive photocathode for PEC application. Our work opens up new opportunities for composite electrode fabrication by exploiting facile candle flame annealing.

CRediT authorship contribution statement

Chunyu Xiao: Conceptualization, Investigation, Writing - original draft. **Bo Lei:** Investigation, Data curation. **Weiliang Jin:** Investigation, Data curation. **Lingling Xu:** Investigation, Funding acquisition, Writing - review & editing.

Declaration of Competing Interest

The authors declare that they have no known competing financial interests or personal relationships that could have appeared to influence the work reported in this paper.

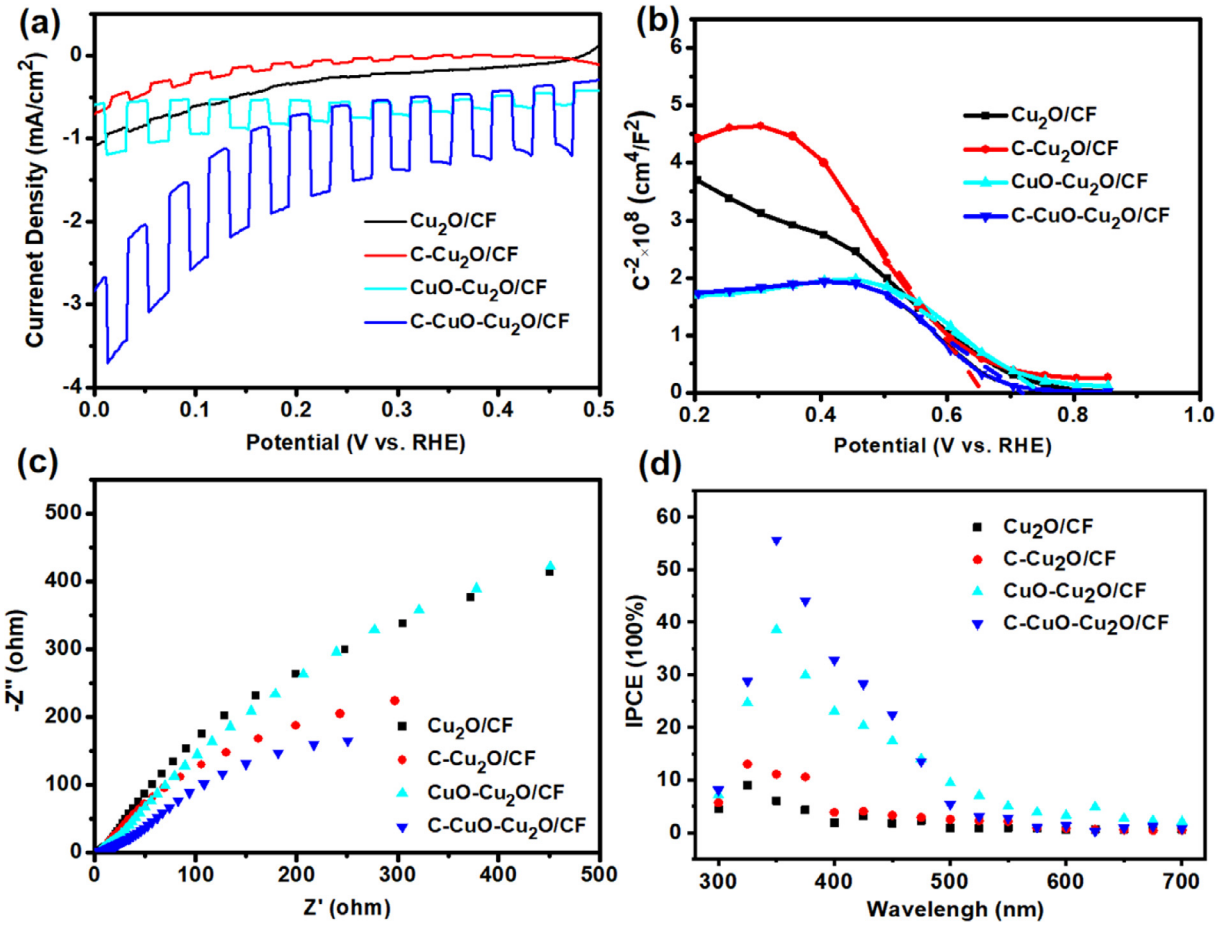

Fig. 3. (a) LSV, (b) M-S plots, (c) EIS and (d) IPCE curves of Cu_2O/CF, C-Cu_2O/CF, CuO-Cu_2O/CF and C-CuO-Cu_2O/CF electrodes.

Acknowledgement

This work was supported by University Nursing Program for Young Scholar with Creative Talent in Heilongjiang Province (UNPYSCT-2015052).

Appendix A. Supplementary data

Supplementary data to this article can be found online at https://doi.org/10.1016/j.matlet.2021.130006.

References

[1] S. Jamali, A. Moshaii, Appl. Surf. Sci. 419 (2017) 269–276, https://doi.org/10.1016/j.apsusc.2017.04.228.
[2] J.Y. Chen, X.L. Liu, H.M. Zhang, Mater. Lett. 182 (2016) 47–51, https://doi.org/10.1016/j.matlet.2016.06.077.
[3] Z. He, Y. Xia, B. Tang, X. Jiang, J. Su, Mater. Lett. 184 (2016) 148–151, https://doi.org/10.1016/j.matlet.2016.08.020.
[4] S. John, S.C. Roy, Appl. Surf. Sci. 509 (2020), https://doi.org/10.1016/j.apsusc.2019.144703 144703.
[5] F. Du, Q. Chen, Y. Wang, J. Phys. Chem. Solids 104 (2017) 139–144, https://doi.org/10.1016/j.jpcs.2016.12.029.
[6] A.A. Dubale, A.G. Tamirat, H.M. Chen, T.A. Berhe, C.J. Pan, W. Su, B. Huang, J. Mater. Chem. A 4 (2016) 2205–2216, https://doi.org/10.1039/c5ta09464j.
[7] L. Yu, G. Li, X. Zhang, X. Ba, G. Shi, Y. Li, P. Wong, J. Yu, Y. Yu, ACS Catal. 6 (2016) 6444–6454, https://doi.org/10.1021/acscatal.6b01455.
[8] X. Liu, Y. Zhang, Y. Jia, J. Jiang, Y. Wang, X. Chen, T. Gui, Chin. J. Catal. 38 (2017) 1770–1779, https://doi.org/10.1016/s1872-2067(17)62888-2.
[9] P.P. Kunturu, J. Huskens, ACS Appl. Energy Mater. 2 (2019) 7850–7860, https://doi.org/10.1021/acsaem.9b01290.
[10] Y. Mao, J. He, X. Sun, W. Li, X. Lu, J. Gan, Z. Liu, L. Gong, J. Chen, P. Liu, Y. Tong, Electrochim. Acta 62 (2012) 1–7, https://doi.org/10.1016/j.electacta.2011.10.106.
[11] P. Chand, A. Gaur, A. Kumar, U.K. Gaur, Appl. Surf. Sci. 307 (2014) 280–286, https://doi.org/10.1016/j.apsusc.2014.04.027.
[12] J.T. Chen, B.J. Yang, H.X. Li, P.J. Ma, J.W. Lang, X.B. Yan, J. Mater. Chem. A 715 (2019) 9247–9252, https://doi.org/10.1039/c9ta01653h.
[13] H. Qi, J. Wolfe, D. Fichou, Z. Chen, Sci. Rep. 6 (2016) 30882, https://doi.org/10.1038/srep30882.